Laser Ablation of Trp-Gly

Jeffrey W. Elam and Donald H. Levy*

Department of Chemistry and the James Franck Institute, University of Chicago, Chicago, Illinois 60637

Received: June 8, 1998; In Final Form: July 13, 1998

We studied laser ablation of Trp-Gly under the same experimental conditions used previously to successfully seed this fragile, nonvolatile dipeptide into a molecular beam. A film of Trp-Gly was prepared on a brass plate and laser ablated with 11 ns, 8 J/cm^2, 5320 Å laser pulses. We found substantial fragmentation upon ablation and believe that immediate helium entrainment is necessary to prevent decomposition. The velocity distribution is broader than a Boltzmann distribution, exhibits no flow velocity, and has a translational temperature $T_t = 4200$ K. The angular distribution is highly forward-peaked and bimodal with a major component proportional to $\cos^{41}\theta$. When laser ablated under identical conditions, tryptamine has a similar angle velocity distribution and also shows significant fragmentation. Analysis of its mass spectrum yields an internal temperature $T_i = 660$ K. Existing collisional models cannot explain the measured angle velocity distributions. They may result from the pulsed nature of the expansion and the finite focused laser spot size.

I. Introduction

Laser desorption is a powerful method for vaporizing large, fragile molecules such as proteins, sugars, and DNA for gas-phase analysis. Two different experimental strategies are typically used to perform laser desorption of organic compounds, and theories have been developed to explain each of them. The first technique, pioneered by Posthumus et al. in 1978,[1] uses a monolayer of transparent sample on a strongly absorbing, metal substrate. It is believed that rapid laser heating of the substrate promotes desorption without fragmentation either by a competing rates process[2] or by an energy bottleneck, which restricts sample heating.[3] The second method, matrix-assisted laser desorption (MALD), was developed by Karas et al. in 1987.[4] MALD employs a thick, strongly absorbing matrix in which is doped a small amount of sample. The success of this method is thought to result from rapid laser heating,[5] photochemical bond cleavage between matrix molecules,[6] or perhaps by a photomechanical process.[7] Rapid collisional cooling in the matrix plume may also prevent sample fragmentation.[8] A recent review[9] details the history, methodology and current understanding of these techniques.

For several years we have been combining laser ablation with supersonic jet spectroscopy to study the electronic spectra of small peptides in the gas phase.[10,11] In this paper, we investigate the properties of a small peptide that has been laser ablated. Many authors have extensively studied laser ablation, and there is a large amount of literature on the subject. We cite here some examples of this literature.[12−19]

In the laser ablation supersonic jet technique,[20] a 5 μm thick, transparent peptide film is prepared on a brass plate by evaporation from methanol solution. The entire irradiated spot of film is removed with each pulse of a 5320 Å, 10^8 W/cm^2 ablation laser. This material ablates into ∼10 atm of helium and expands into the vacuum as a supersonic jet. Figure 1 illustrates the utility of this method. When Trp-Gly is heated in a 270 °C oven, the resulting mass spectrum (Figure 1a) shows no intensity at the parent mass (261 amu) and a large fragment peak at the indole mass (117 amu). Figure 1b, recorded using the supersonic expansion laser ablation source, shows almost no fragmentation and a strong parent peak. The advantage of this technique over those described above is that neutral sample molecules are formed in sufficient abundance and with sufficient shot-to-shot stability to allow spectroscopy. The mechanism responsible for this process is not known. The objective of this study is to reproduce these sample preparation and ablation conditions in order to understand the mechanism behind the laser ablation supersonic jet technique. In the present investiga-

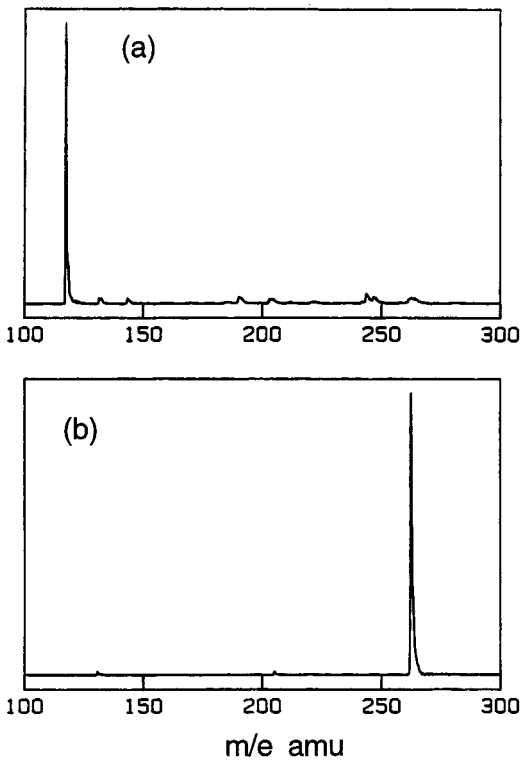

Figure 1. Mass spectra of Trp-Gly obtained using two different vaporization techniques. (a) shows the mass spectrum recorded when Trp-Gly is heated in a conventional oven source to 270 °C. (b) is recorded using the supersonic expansion laser ablation source. These figures are taken from ref 20.

S1089-5647(98)02545-0 CCC: $15.00
Published on Web 09/19/1998

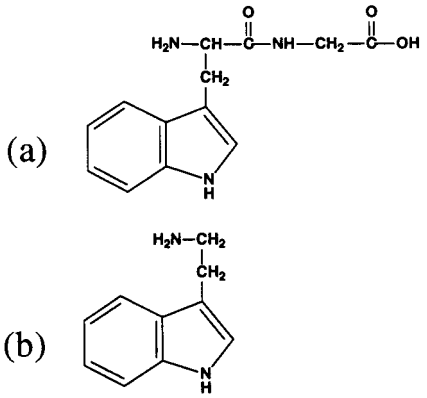

Figure 2. Molecular structures of (a) Trp-Gly and (b) tryptamine.

tion, ablation is performed without helium entrainment to allow measurements on the nascent, ablated material.

We chose Trp-Gly as a model compound in this study for a number of reasons. Peptides containing the amino acid tryptophan bear the indole chromophore and are efficiently ionized by resonantly enhanced two-photon ionization (R2PI). Trp-Gly is the smallest and therefore simplest tryptophan containing peptide. Nevertheless, Trp-Gly is sufficiently nonvolatile that it cannot be vaporized by conventional means. Its fragility causes it to fragment when heated, making it a convenient probe of harsh conditions. Not surprisingly, dipeptides are often used as test compounds for developing new methods of sample introduction.[21] Additionally, the electronic spectroscopy of Trp-Gly is known.[10]

In addition to Trp-Gly (Figure 2a), tryptamine (Figure 2b) was studied to probe the degree of internal excitation achieved in the ablation process. Tryptamine has a mass spectral fragment whose metastable decay rate as a function of internal energy is known,[20] so by measurment of this rate, the internal temperature can be deduced. We cannot apply this method to Trp-Gly directly, since it has no known metastable fragments. This technique was used previously to measure the internal temperature of alkylamines vaporized by MALD.[22]

II. Experiment

The apparatus used for performing these experiments has been described previously.[23] The principle components (Figure 3) are a translatable sample plate and position-sensitive detector (microchannel plate, MCP) housed in a diffusion-pumped, high-vacuum chamber and two 10 ns lasers for ablation and R2PI. The ablation laser strikes the sample plate along the surface normal, generating an expanding plume of neutral molecules. After delay t, the ionization laser fires (perpendicular to the page in Figure 3), creating a line of ions parallel to the MCP at a distance d from the sample plate. The resulting photoions have a velocity component perpendicular to the sample plate $v_z = d/t$. These ions are accelerated away from the grid and strike the MCP after a flight time determined by their mass-to-charge ratio, m/e. The output of the MCP is coupled to a phosphor. By temporal resolution of this signal with a phototube (PMT), the mass spectrum of laser-ablated material is measured. The angular distribution for a given mass is obtained by gating the MCP on that mass and capturing an image of the phosphor with a video camera. A sequence of video images measured at various t is transformed into an angle velocity distribution.

Sample films of either Trp-Gly or tryptamine (Sigma) were prepared by dissolving 30 mg of these compounds in 15 mL of a 1:1 mixture of methanol and water, pouring the entire solution

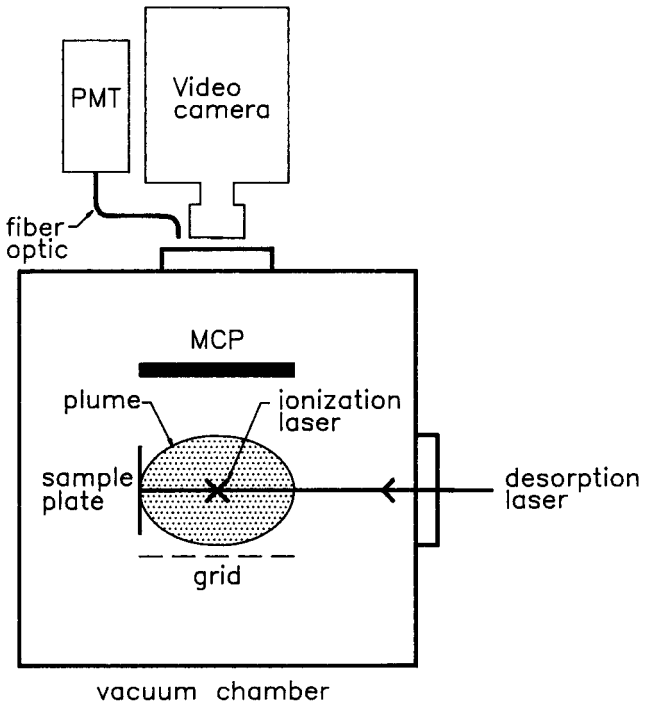

Figure 3. Side view schematic of laser ablation apparatus.

onto a brass plate, and gently heating to evaporate the solvent. In addition to the 30 mg of sample, the solutions contained 0.020 mg of trifluoroacetic acid, 0.50 mg of a methanol solution of surfactant (FC431, 3M), and, for films containing laser dye, 0.050 mg of rhodamine 6G (R6G.) Trifluoroacetic acid prevented tryptamine films containing R6G from becoming colorless when dried. The surfactant improved film uniformity. The sample plate was continuously translated such that each ablation laser pulse struck fresh film. The plate could be cooled with a cold tip to 120 K.

The sample film thickness was measured with an optical microscope to be 7($\pm$2) μm. In addition, the film thickness may be estimated from $t = m/(dA)$, where m is the mass of Trp-Gly present in the film ($m = 30$ mg), d is the density of Trp-Gly ($d \approx 1.2$ g/cm^3), and A is the area of the film ($A = 52$ cm^2). The estimated film thickness is $t = 5$ μm, in good agreement with the measured film thickness of 7($\pm$2) μm.

The ablation laser was the second harmonic of a Spectra Physics DCR1 YAG (10 Hz, 11 ns fwhm, 5320 Å). The central, most spatially homogeneous portion of this beam was selected with an iris, attenuated to $E = 0.04-0.50$ mJ/pulse, and focused onto the sample plate with an $f = 31$ cm lens. The focused spot size was 2×10^{-5} cm^2 as determined with a pinhole profiler and by examination of melt pits in gold foil.[24] The ionization laser was a frequency-doubled, excimer-pumped coumarin 540A dye laser tuned to 2863 Å for tryptamine[25] and 2865 Å for Trp-Gly.[10]

III. Results

Preliminary measurements confirmed the location of initial ablation laser energy deposition and the nonvolatility of Trp-Gly. First, a neat (no R6G) Trp-Gly film was prepared on a quartz plate at 290 K and laser ablation was attempted at laser energies between 0 and 1.5 mJ/pulse. No signal was observed from Trp-Gly or fragments. The damage threshold measured for quartz using our laser and focusing conditions is 1.2 mJ/pulse. Second, a neat Trp-Gly film on brass was resistively heated to 565 K while monitoring the mass spectrum of the

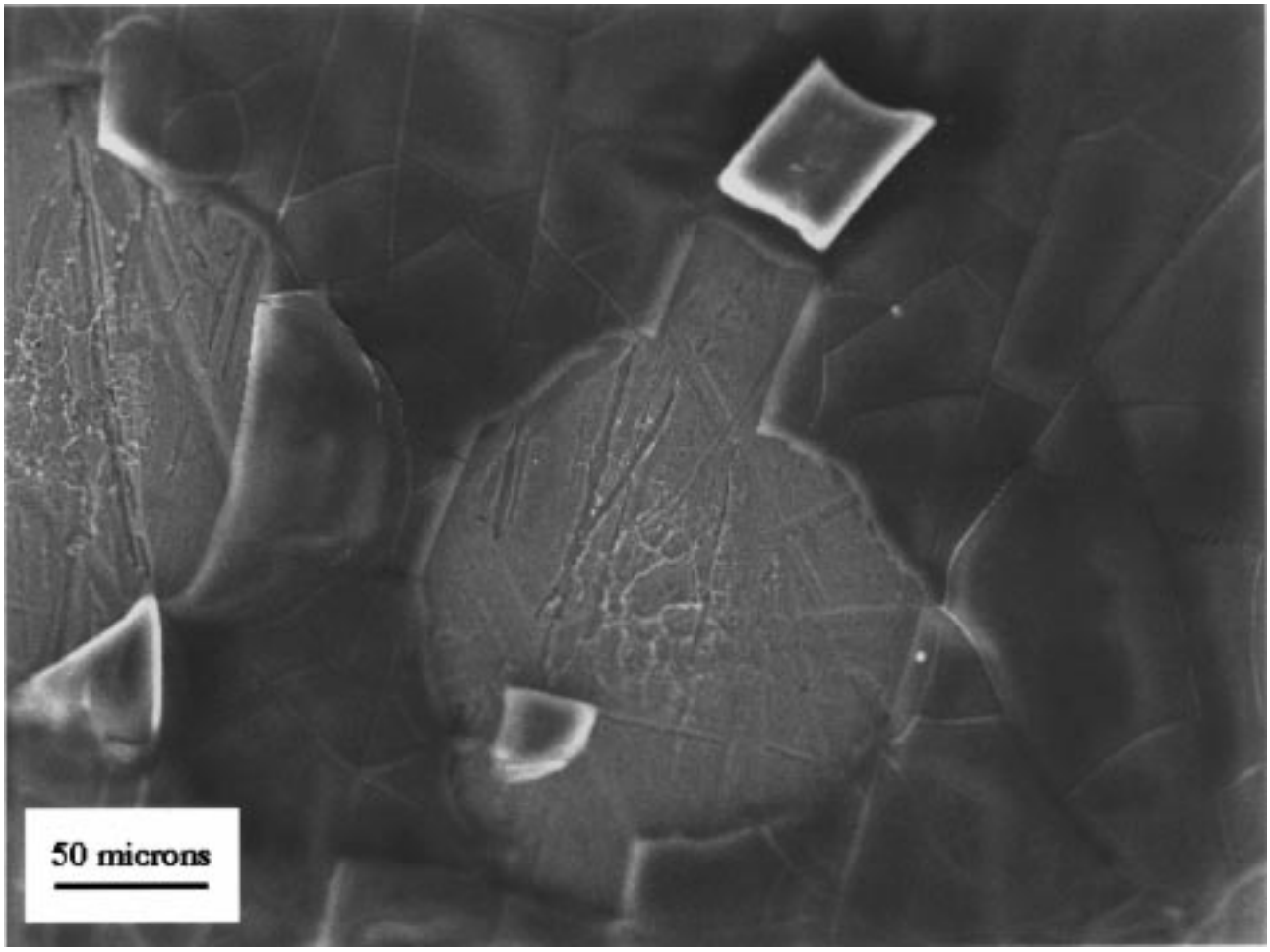

Figure 4. SEM image of laser-ablated Trp-Gly film.

vaporized material. Although large fragment signals were observed at masses 117, 131, 160, and 258 amu, no Trp-Gly signal was seen at $m = 261$ amu.

Figure 4 is a scanning electron microscope (SEM) image showing the effects of ablation on the sample film and brass plate. In the center is an irregularly shaped ablation spot approximately 150 μm in diameter from which all of the Trp-Gly is gone, revealing the underlying brass. Also shown is a portion of an adjacent spot from a different laser pulse. Clearly, some of the film ablates as large chunks (tens of micrometers), which break along cracks in the film. These cracks are present in regions of the film unexposed to the ablation laser. The ablated spot size increases with ablation laser energy. Under an optical microscope, the whitened area near the center of the spot is revealed to be a 50 μm diameter melt crater in the brass. Although these craters have a uniform shape from shot to shot, the surrounding regions of ablated film vary in shape.

We measured ablation laser threshold energies by gating the MCP on the parent ion mass and gradually increasing the ablation laser energy until signal was observed. The results were $E = 0.079$ mJ/pulse for Trp-Gly with and without R6G at 290 K, $E = 0.12$ mJ/pulse for neat Trp-Gly at 120 K, and $E = 0.10$ mJ/pulse for neat tryptamine at 290 K. The uncertainty for these threshold measurements is $\pm 20\%$.

Figure 5 is a mass spectrum recorded from a Trp-Gly film with R6G at $T = 290$ K, $E = 0.24$ mJ/pulse, and $v_z = 550$ m/s. The mass peaks in amu and the relative intensities are 261(64), 246(49), 160(25), 143(22), 131(100), and 117(31). As the ablation laser energy is increased from threshold to 4 times threshold, the parent mass signal at 261 amu increases monotonically and approximately linearly and the fragmentation pattern remains relatively constant. The behavior of neat films and films with R6G is the same, but when the plate temperature is reduced to 120 K, the signal is reduced.

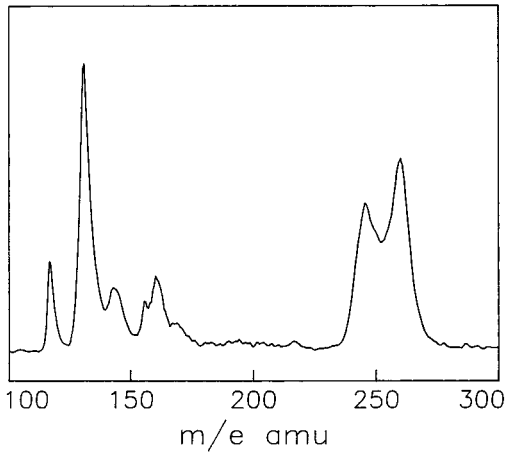

Figure 5. Mass spectrum of Trp-Gly laser ablated without helium entrainment. The sample was Trp-Gly with R6G at $T = 290$ K, $E = 0.24$ mJ/pulse, and $v_z = 550$ m/s.

Figure 6 depicts surface and contour plots for an angle velocity distribution of laser-ablated Trp-Gly with R6G at $T = 120$ K and $E = 0.32$ mJ/pulse. θ is the angle between the ablating particle velocity vector and the sample plate normal. The angular distribution is extremely forward-peaked and symmetric about the surface normal. The velocity distribution has a single, broad peak at 450 m/s. Figure 7a shows the

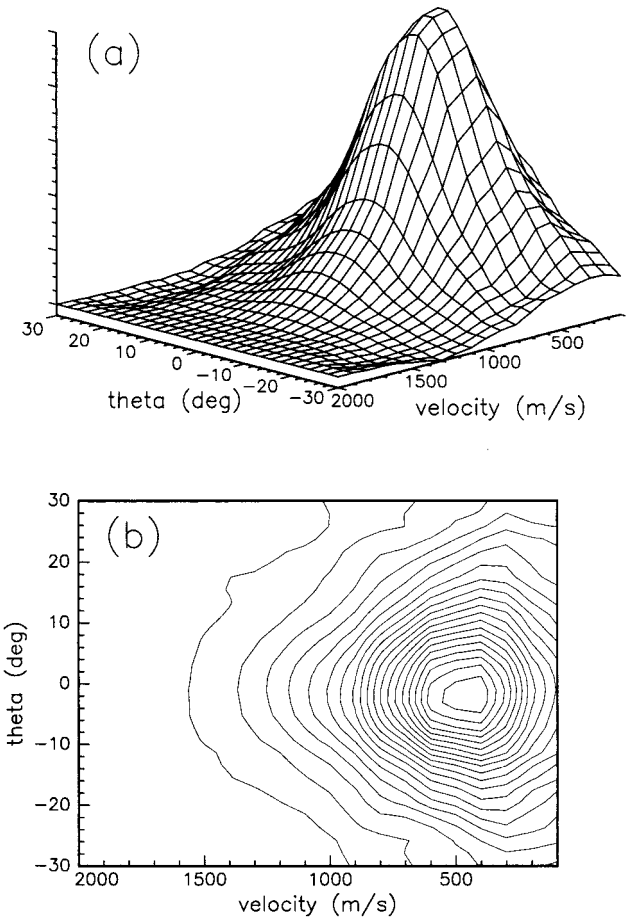

Figure 6. Surface (a) and contour plots (b) of angle velocity distribution of laser-ablated Trp-Gly. The film was Trp-Gly with R6G at $T = 120$ K and $E = 0.32$ mJ/pulse.

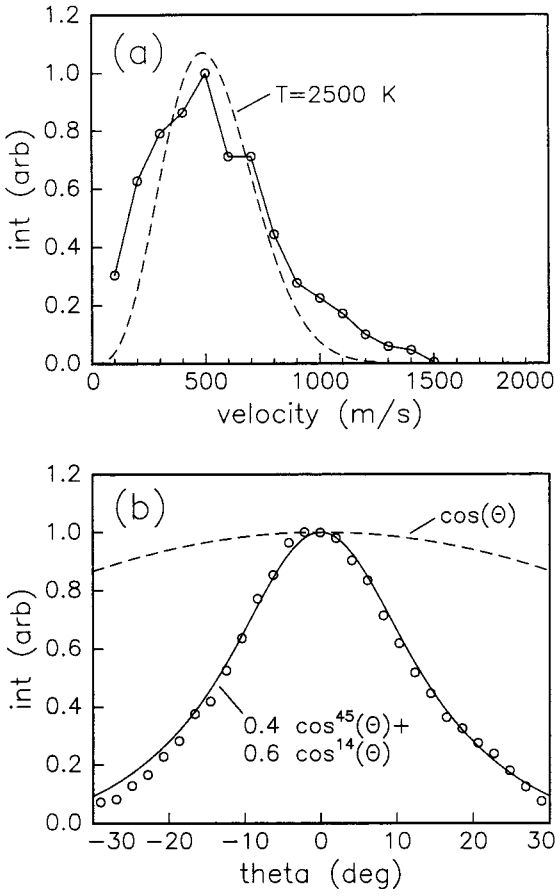

Figure 7. Velocity distribution (a) and angular distribution (b) of laser-ablated Trp-Gly. These plots result from the same data set as that used in Figure 6. The dashed line in (a) is a Boltzmann flux distribution at $T = 2500$ K. The solid line in (b) is a fit to the data using the function indicated while the dashed line is a cos θ distribution.

velocity distribution that results from binning the data of Figure 6 along the θ axis. The circles and solid line represent data, while the dashed line results from a fit using a Boltzmann flux distribution

$$y = Av^3 \exp\left(\frac{-mv^2}{2kT}\right) \tag{1}$$

varying A and T, where v is velocity, m is mass, T is temperature, and k is the Boltzmann constant. The results are $A = 0.41 \times 10^{-7}$ and $T = 2500$ K. The experimental velocity distribution is broader than a Boltzmann distribution. Inclusion of a flow velocity[26] in eq 1 does not improve the fit.

Figure 7b depicts the angular distribution that results from binning the data of Figure 6 along the velocity axis. The circles represent data, and the solid line results from a fit using

$$y = A \cos^m \theta + (1 - A) \cos^n \theta \tag{2}$$

varying A, m, and n. The results are $A = 0.4$, $m = 45$, and $n = 14$. For comparison, the dashed line shows $y = \cos \theta$ ($A = 1$, $m = 1$ in eq 2) as would result from collisionless, thermal desorption.

Table 1 summarizes the angle velocity distributions measured. The first column lists the molecule studied and whether the film contains R6G. The next three columns list the plate temperature, mass monitored, and ablation laser energy used. The columns titled A, m, and n result from eq 2. The columns titled $\langle|\theta|\rangle$, $\langle v\rangle$, and T_t list the average absolute angle, average velocity, and translational temperature ($T_t = \langle E_t\rangle/(2k)$). The angle and velocity distributions do not change dramatically with any of the parameters varied. In particular, parent and fragment distributions are nearly identical. The similarity between the tryptamine and Trp-Gly data supports the use of tryptamine as an internal energy probe. Some small systematic trends were observed: both $\langle v\rangle$ and T_t increase and $\langle|\theta|\rangle$ decreases with either E or inclusion of R6G. Some of these changes are within the uncertainty of the measurements ($\pm$20% for $\langle v\rangle$, $\pm$5% for $\langle|\theta|\rangle$) and may or may not be real.

Figure 8b depicts a time-of-flight mass spectrum obtained from laser-ablated tryptamine with R6G at $T = 290$ K, $E = 0.17$ mJ/pulse, and $v_z = 610$ m/s. Figure 8a is a background spectrum measured under identical conditions but with the ablation laser blocked. The background spectrum exists because of the room-temperature vapor pressure of tryptamine. Both spectra show the parent peak at 5.29 μs (160 amu) and a fragment at 4.79 μs (131 amu.) The ratio of fragment to parent in the laser ablation spectrum (0.36) is higher than that in the background (0.091). The fragment peak in Figure 8b is broadened toward longer flight times relative to that of the parent. Figure 9 is an expanded view of Figure 8b. The small shoulder visible on the 4.79 μs peak at 4.77 μs (130 amu) increases with respect to the 4.79 μs peak as the ionization laser power increases. The solid line results from a fit to the 4.79 μs peak using an exponential decay with constant $k' = 8.2 \times 10^6$ s^{-1}.

TABLE 1. Summary of Angle and Velocity Distributions

film[a]	T[b] (K)	*m*[c] (amu)	*E*[d] (mJ/p)	A[e]	m	n	$\langle\|\theta\|\rangle$[f] (deg)	$\langle v\rangle$[g] (m/s)	T_t[h] (K)
Trp-Gly, R6G	290	261	0.16	0.57	54	4.5	11	440	1900
Trp-Gly, R6G	290	261	0.24	0.59	45	9.9	10	560	3100
Trp-Gly, R6G	290	131	0.24	0.53	33	1.0	13	570	1900
Trp-Gly, R6G	120	261	0.24	0.61	37	2.3	12	470	2400
Trp-Gly, R6G	120	261	0.32	0.43	55	14	10	550	2900
Trp-Gly, neat	290	261	0.16	0.57	41	8.4	10	670	4200
Trp-Gly, neat	290	261	0.24	0.61	47	10	9.0	720	5000
Trp-Gly, neat	290	131	0.24	0.62	45	6.0	11	820	3200
tryptamine, neat	290	160	0.17	0.46	24	10	11	600	1900

[a] Molecule comprising film. R6G indicates that the film contains 0.1% laser dye; neat implies that it does not. [b] Temperature of sample plate. [c] Mass monitored during angle, velocity scan. [d] Ablation laser energy. [e] Columns *A*, *m*, and *n* result from a fit to the angular distribution using eq 2. [f] Average of absolute value of angular distribution. [g] Average value of velocity distribution. [h] Translational temperature $T_t = \langle E_t\rangle/(2k)$.

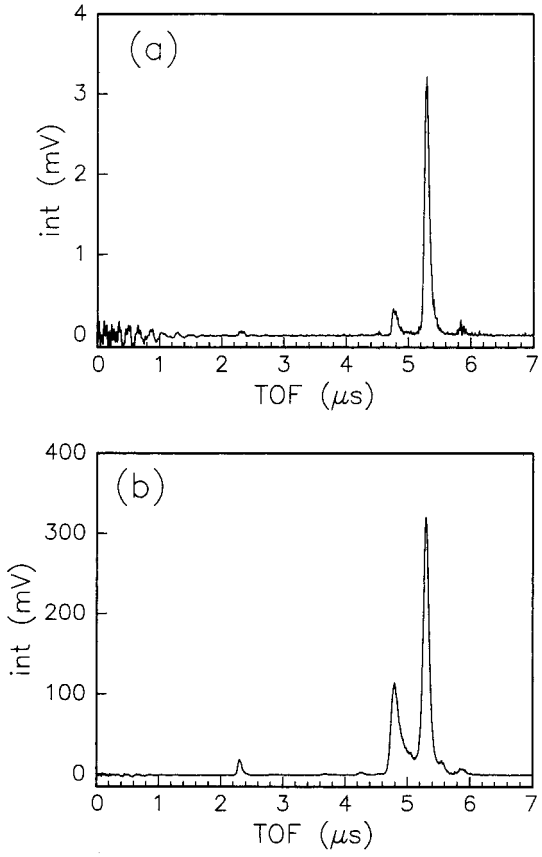

Figure 8. Time-of-flight mass spectra of tryptamine. (a) is a background spectrum measured with the ablation laser blocked, while (b) results from laser ablation.

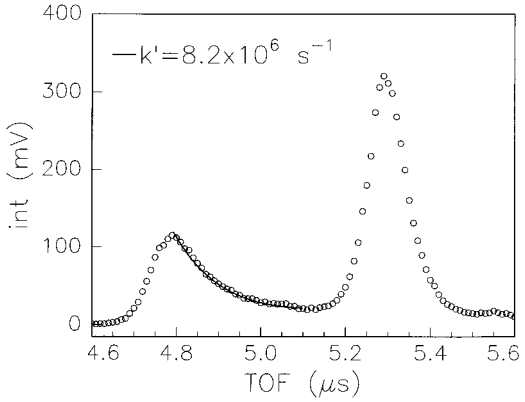

Figure 9. Expanded view of the time-of-flight spectrum of laser-ablated tryptamine. The circles represent the same data as that shown in Figure 8b, while the solid line results from a fit to the 4.79 μs metastable mass peak using an exponential decay. The resulting decay constant is indicated.

IV. Discussion

Attempts to explain laser ablation experiments often divide the phenomenon into two phases: (1) the initial vaporization process and (2) the process of gas-phase collisions following vaporization. The effect of the second, collisional phase is to modify the nascent angle, velocity, and internal energy distributions, and hence dynamical information may be obscured. For example, a $\cos^5\theta$ angular distribution is clear evidence for a nonthermal vaporization process if gas-phase collisions are rigorously excluded.[27] However, since the same distribution results from a thermally ablated sample experiencing two to three collisions per particle,[28] little can be said about the initial vaporization process (phase 1) if the extent of collisional perturbation (phase 2) is uncertain. This convolution complicates interpretation in the current study.

Several models address the first phase of the ablation process and the choice of which is appropriate depends on the initial site of laser energy deposition, the sample film or the underlying substrate. The failure to observe laser ablation from a transparent substrate (quartz) along with the production of melt craters on a strongly absorbing substrate (brass) suggest that laser energy is deposited in the substrate.

One puzzling finding relates to the inclusion of R6G. Tubergen found more than an order of magnitude increase in signal and an order of magnitude decrease in ablation threshold from films containing 0.003 M R6G.[20] At this concentration, Tubergen's 5 μm films absorbed ~30% of the ablation laser energy. In the present study, the films with R6G absorbed ~40% of the ablation laser energy. The resulting temperature rise in the film may be estimated from $\Delta T = Es/n$, where E is the absorbed laser energy ($E = 3 \times 10^{-5}$ J at threshold), s is the heat capacity ($s \approx 0.5$ J g^{-1} K^{-1}), and n is the mass of irradiated material ($n = 1.5 \times 10^{-8}$ g). Thus $\Delta T \approx 1000$ K. This estimate ignores thermal diffusion; however, the thermal diffusion length of solid, organic films is very small[23] and the brass substrate is expected to be hotter than the film (section IV.A). $\Delta T \approx 1000$ K suggests that R6G in the films should greatly affect the ablation process. However, the only changes seen upon addition of R6G were perhaps a small decrease in $\langle v\rangle$ and a small increase in $\langle|\theta|\rangle$ (Table 1).

The simplest model for desorption from an absorbing substrate is laser heating followed by thermal evaporation; however, this does not explain why desorption occurs without fragmentation. Two models that account for this are the energy bottleneck model of Zare and Levine[3] and the competing rates model of Hall and DeSantolo.[2] One method for differentiating between these models is to compare the temperatures of different degrees of freedom of the desorbing molecules. Since the

competing rates model assumes equilibrium, the internal and translational temperatures should equal the surface temperature at the moment of desorption. The bottleneck model predicts the internal temperature to be lower than the surface temperature at desorption.

There have been several recent measurements of the internal energy of laser desorbed molecules.[29−31] Unfortunately, these studies do not conclusively settle the question of whether there is or is not a bottleneck to internal heating of the desorbed molecule. In addition, the results for laser-ablated peptides reported here need not be the same as those for laser-desorbed material reported previously.

Several models address the second, collisional phase of the ablation process. Knudsen layer theory asserts that when the ablation laser energy is sufficiently high to remove approximately 1 monolayer (ML) per 10 ns pulse, a $\cos^4\theta$ angular distribution and flow velocity, u, equaling the local speed of sound result (so that the mach number $M = 1$). Additionally, there is a weak dependence of the velocity distribution on angle, with the peak velocity at $\theta = 75°$ only 0.8 times the peak velocity at $\theta = 0°$. At higher ablation laser energy, the ablated plume undergoes unsteady adiabatic expansion.[32] The angular distribution narrows, ($\cos^p\theta$ where $p \approx (1 + M)^2$), u and M increase, the translational temperature decreases, and the dependence of the velocity distribution on angle strengthens. These trends continue as long as the plume density remains sufficiently high to support collisions.

In both the Knudsen layer and unsteady adiabatic expansion models, laser energy is the critical parameter in determining the final distributions. In the hydrodynamical model,[33] the important parameters are the focused laser spot size and the height of the laser-generated plume at the onset of 3D expansion, while laser energy is immaterial to first order. This model predicts that collisions will transform any initial angle velocity distribution into an elliptical Boltzmann distribution with a flow velocity. The angular distribution will be approximately $\cos^p\theta$; however, increased intensity at large angle relative to this functional form is predicted.

While the effect of collisions on internal energy is not addressed in these models, the expectation is that collisions will transfer energy from internal modes into directed flow. The extent of cooling will depend on the number of collisions per particle and on the R−T and V−T collision numbers. This expectation is corroborated by Monte Carlo simulation[34] and by a wealth of literature regarding supersonic jets.[35]

IV.A. SEM and Sample Observations. A significant parameter in evaluating the ablation process is the peak substrate temperature, since (for thermal processes) it establishes the initial distributions and determines the extent of collisional effects. Craters formed in the brass plate by single laser pulses are likely produced by thermal evaporation, since other known mechanisms of laser metal sputtering (hydrodynamic, exfoliational) require multiple pulses on the same spot.[36] This suggests a peak substrate temperature above the boiling point. We estimate the peak brass surface temperature, T_f, at threshold energy from[37]

$$\Delta T = \frac{8}{3}\left(\frac{1}{(4 - t_r)/t_0}\right)^{1/2}\left(\frac{F_0}{K}\right)\left(\frac{\kappa t_0}{\pi}\right)^{1/2}$$

ΔT is the rise in surface temperature, t_0 and t_r are the fwhm and rise time of the laser pulse, F_0 is the peak absorbed laser power density, K is the thermal conductivity, and κ is the thermal diffusivity. Using appropriate thermal[38] and optical[39] parameters, $T_f = 3000$ K. This calculation of ΔT assumes that the thermal and optical parameters remain constant with temperature and that heat flows one-dimensionally from the surface into the solid. While the boiling point of brass is unknown, it probably lies between those of copper (2840 K) and zinc (1180 K). Hence, even at threshold energy, the brass is raised above its boiling point where evaporation is efficient. One explanation for the appearance of large sample chunks (Figure 4) is that high pressure from evaporated metal vapor causes the film to rupture explosively, liberating large flakes that break preferentially along preexisting cracks.

IV.B. Mass Spectra and Internal Energy. The fragmentation pattern for laser-ablated Trp-Gly resembles those measured under higher mass resolution in both pulsed rapid heating[40] and in CO_2 laser ablation experiments.[40,41] The observation that both tryptamine and Trp-Gly fragment when ablated indicates that a large amount of internal energy is acquired during ablation. The internal temperature may be deduced from the tryptamine mass spectrum. This analysis is facilitated by a previous study of jet-cooled tryptamine photofragmentation under higher mass resolution.[20] This work found that while absorption of two UV photons forms the parent ion at $m = 160$ amu, three and four photon absorption form fragments at $m = 131$ amu and $m = 130$ amu, respectively. The degree of fragmentation increases with ionization laser power density. The $m = 131$ amu peak results from a metastable fragment formed by unimolecular dissociation of the parent ion on a microsecond time scale. The $m = 130$ amu peak is a prompt fragment. Both are thought to form through cleavage of the alkyl chain at the second carbon atom from the aromatic rings followed by rearrangement.

The signature of a metastable peak in the time-of-flight mass spectrum is a broadening toward longer flight times.[42] The unimolecular decay rate constant can be extracted from the exponential decay of such a metastable peak. Tubergen measured the rate constant of tryptamine as a function of excess internal energy by analyzing the $m = 131$ amu peak from a series of mass spectra acquired at increasing ionization laser photon energy. The result obtained in the range 5.3−6.7 eV is

$$\ln[k(E)] = 1.09E + 6.73 \qquad (3)$$

with E in eV and k in s^{-1}. This value for k is reportedly accurate within a factor of 2.

Since the ionization laser wavelength and power density are identical for Figures 8a and 8b, the fragmentation patterns indicate a difference in the samples probed. There are two explanations for the fact that the $(m = 131)/(m = 160)$ peak intensity ratio is nearly 4 times larger for the laser ablation mass spectrum than for the background mass spectrum: either the material is already fragmented when probed or a larger fraction fragments between ionization and detection. In either case, the tryptamine has ablated hot relative to the background (room temperature) sample. Evidence for the latter explanation is the metastable broadening seen on the $m = 131$ amu peak in Figure 8b. Although our mass resolution is insufficient to resolve $m = 130$ amu from $m = 131$ amu, the relative increase of the $m = 130$ amu shoulder with laser power supports the assignment of the $m = 131$ amu peak as the metastable fragment ion.

The metastable fragmentation rate for laser-ablated tryptamine can be determined from the 4.79 μs (131 amu) peak of Figure 9. This peak can be fit with an exponential decay with the rate constant $k' = 8.2 \times 10^6\ s^{-1}$. The units for this rate constant must be converted from time-of-flight to time-of-reaction.[42] For our instrument, this relationship is linear and $k = 0.14k'$ at the mass spectrometer voltages used for Figure 9. Thus $k = 1.1 \times$

10^6 s^{-1}, and from eq 3, the excess energy is $E = 6.7$ eV. The energy supplied is three 2863 Å photons (13.02 eV) minus the tryptamine ionization potential (7.69 ± 0.08 eV)[43] or 5.3 eV. Hence, the internal energy present before laser excitation is $E_i = 1.4$ eV. By application of group additivity rules to tabulated heat capacity values,[44] we estimated the temperature-dependent heat capacity for tryptamine, numerically integrated, and inverted this to yield $T_i(E_i)$, from which $T_i = 660(\pm 110)$ K.

Comparison of Figures 1b and 5 shows a striking result of this study. Both are mass spectra of laser-ablated Trp-Gly yet Figure 5 shows extensive fragmentation and Figure 1b does not. The only experimental difference is that in Figure 1b, the sample ablated into 10 atm of helium and then expanded supersonically, whereas in Figure 5, the sample ablated into a vacuum. One explanation is that in both cases, Trp-Gly ablates hot; however, in the first case, these molecules rapidly cool to room temperature by collisions with helium, while in the second case the Trp-Gly remains hot throughout its trajectory to the detector. During this time (~100 μs), many parent molecules undergo unimolecular dissociation.

This explanation requires that the time for vibrational relaxation in the helium bath, t_v, is smaller than that for unimolecular dissociation, t_d. To estimate t_v, we begin with the collision frequency, $Z = \sigma C_{rel} n$, where σ is the relative collisional cross section, C_{rel} is the average relative velocity, and n is the number density of helium at 10 atm and room temperature. Assuming $\sigma = 1.0 \times 10^{-14}$ cm^2, $Z = 3.1 \times 10^{11}$ s^{-1}. During collisional cooling, the internal energy versus time is[45] $d\langle E\rangle/dt = -Z\langle \Delta E\rangle$, where $\langle E\rangle$ is the internal energy and $\langle \Delta E\rangle$ is the average energy transferred per collision between vibrationally excited Trp-Gly and helium atoms. While this quantity is unknown, the value for toluene at $\langle E\rangle = 52\,000$ cm^{-1} is $\langle \Delta E\rangle = 75$ cm^{-1}.[46] Assuming a similar value for Trp-Gly and also a linear dependence between $\langle \Delta E\rangle$ and $\langle E\rangle$,[45,47] Trp-Gly will cool by 90% in time $t_v = 5$ ns.

To estimate t_d, we assume that Trp-Gly ablates at the same temperature as tryptamine, 660 K. Using an upper limit heat capacity of $^1/_2kT$ per internal mode, $\langle E\rangle = 3$ eV. When eq 3 is applied, $k = 2 \times 10^4$ s^{-1}. This estimate is conservative by RRKM theory, since Trp-Gly has ~50% more vibrational modes than tryptamine and since one expects the neutral to have a higher dissociation energy than the ion. Within $t_d = 100$ μs 90% fragmentation will occur. Thus, $t_v \ll t_d$, justifying this collisional cooling model.

Recently, several authors[40,48] have studied the role of supersonic jet cooling on the fragmentation of thermally labile organic compounds vaporized by laser ablation. In these experiments, laser ablation mass spectra were recorded with and without supersonic expansion, and in each case, the fragmentation pattern was relatively unaffected. However, in both of these studies, carrier gas entrainment occurs after laser ablation. It is possible that most fragmentation occurs before the laser-ablated compounds encounter the carrier gas, and thus, supersonic cooling has little effect.

IV.C. Velocity Distributions. Our velocity distributions do not match the predictions of existing collisional models. One expects gas-phase collisions to generate a narrow velocity distribution that is faster at smaller angles and has positive flow. Our distributions are broader than a Boltzmann distribution, independent of angle, and exhibit zero flow. Since collisional effects cannot be deconvoluted from the velocity distributions, we cannot extract a nascent translational temperature with which to analyze the initial ejection mechanism.

One explanation for the broad distributions is the pulsed nature of the expansion. Particles in the early and late stages of the gas cloud experience fewer collisions, and hence, their final velocity distribution is different from that in the middle of the cloud. This results in an ensemble of velocity distributions whose sum is broader than its components. Although this effect was not observed in the Monte Carlo simulations of NoorBatcha et al., they examined only the low ablation yield limit (~0.8 ML per pulse). Perhaps a higher initial gas-phase density is required for this broadening effect to manifest. In a more recent simulation[49] at higher yield (2.5 ML per pulse), broadening was seen. These authors cite the pulsed nature of the expansion as the cause.

IV.D. Angular Distributions. Collisions may explain our highly forward-peaked angular distributions and the fact that $\langle|\theta|\rangle$ decreases slightly with laser energy. The weak dependence of the measured angular distributions on laser energy agrees with the hydrodynamical model. However, our angular distributions deviate farther from $\cos^p\theta$ than is predicted by this model and are fit more satisfactorily by eq 2. A bimodal angular distribution consisting of a forward-peaked component ($p > 11$) and a broad component ($p = 1$) was measured previously for an excimer-laser-ablated high-temperature superconductor.[50] The authors attributed the forward-peaked component to adiabatic expansion and the broad component to collisionless, thermal evaporation. In our angular distributions, all films save one (row 3 of Table 1) had $p > 1$ for both components. Since p is extremely sensitive to collisions, collisionless, thermal evaporation is ruled out.

Kelly suggests that a bimodal angular distribution may result from the finite spot size and Gaussian profile of the vaporization laser. These factors will cause molecules near the periphery of the ablation plume to pass from adiabatic expansion into free flight sooner than those near the center and, hence, become less forward-peaked. However, Sibold and Urbassek did not observe this effect in their simulations.

The similarity between the angular distributions for $m = 131$ amu and $m = 261$ amu in laser-ablated Trp-Gly suggests that both measurements probe the same collection of hot molecules. Thus the $m = 131$ amu signal arises from those molecules that undergo unimolecular fragmentation between ablation and detection. The fact that the fragment angular distributions are slightly broader than those of the parent may be because these molecules travel in a more rarefied region of the plume, where collisional cooling is less effective and angular forward-peaking is less pronounced. Alternatively, this difference may stem from transverse velocity imparted to the fragments upon dissociation.

V. Summary

Using the laser ablation technique studied here, molecules ablate hot and, unless rapidly cooled by helium entrainment, many fragment. Tryptamine laser ablates with an internal temperature $T_i = 660(\pm 110)$ K. The measured angular distributions are extremely forward-peaked and bimodal; the velocity distributions are broader than a Boltzmann distribution and exhibit no flow velocity. The failure of existing collisional models to describe our data may result from simplifying assumptions that are violated in our experiment—the broad velocity distributions may result from the pulsed nature of the expansion, and the bimodal angular distributions may result from the finite laser spot size. Monte Carlo simulation could evaluate these hypotheses.

Acknowledgment. This work was supported by the NSF under Grant No. CHE-9319958 and, in part, by the MRSEC program of the NSF under Grant No. DMR-9400379.

References and Notes

(1) Posthumus, M. A.; Kistemaker, P. G.; Meuzelaar, H. L. C.; Ten Noever de Brauw, M. C. *Anal. Chem.* **1978**, *50*, 985.
(2) Hall, R. B.; DeSantolo, A. M. *Surf. Sci.* **1984**, *137*, 421.
(3) Zare, R. N.; Levine, R. D. *Chem. Phys. Lett.* **1987**, *136*, 593.
(4) Karas, M.; Bachmann, D.; Bahr, U.; Hillenkamp, F. *Int. J. Mass. Spectrom. Ion Processes* **1987**, *78*, 53.
(5) Vertes, A.; Gijbels, R.; Levine, R. D. *Rapid Commun. Mass Spectrom.* **1990**, *4*, 228.
(6) Garrison, B. J.; Srinivasan, R. *J. Appl. Phys.* **1985**, *57*, 2909.
(7) Williams, P.; Sundqvist, B. *Phys. Rev. Lett.* **1987**, *58*, 1031.
(8) Vertes, A.; Irinyi, G.; Gijbels, R. *Anal. Chem.* **1993**, *65*, 2389.
(9) Levis, R. J. *Annu. Rev. Phys. Chem.* **1994**, *45*, 483.
(10) Cable, J. R.; Tubergen, M. J.; Levy, D. H. *J. Am. Chem. Soc.* **1988**, *110*, 7349.
(11) Cable, J. R.; Tubergen, M. J.; Levy, D. H. *J. Am. Chem. Soc.* **1989**, *111*, 9032.
(12) Srinivasan, R. *Science* **1986**, *234*, 559.
(13) Chuang, T. J. *Surf. Sci. Rep.* **1983**, *3*, 1.
(14) Dutoit, B.; Zeisel, D.; Decket, V.; Zenobi, R. *J. Phys. Chem. B* **1997**, *101*, 6955.
(15) Cousins, L. M.; Levis, R. J.; Leone, S. R. *J. Chem. Phys.* **1989**, *91*, 5731.
(16) Buck, M.; Hess, P. *Appl. Surf. Sci.* **1989**, *43*, 358.
(17) Zhigilei, L. J.; Kodali, P. B. S.; Garrison, B. J. *J. Phys. Chem. B* **1997**, *101*, 2028.
(18) Zhigilei, L. V.; Garrison, B. J. *Appl. Phys. Lett.* **1997**, *71*, 551.
(19) Srinivasan, R.; Braren, B. *Chem. Rev.* **1989**, *89*, 1303.
(20) Tubergen, M. J. Ph.D. Thesis, University of Chicago, 1991.
(21) Li, L.; Hogg, A. M.; Wang, A. P. L.; Zhang, J. Y.; Nagra, D. S. *Anal. Chem.* **1991**, *63*, 974.
(22) Mowry, C. D.; Johnston, M. V. *J. Phys. Chem.* **1994**, *98*, 1904.
(23) Elam, J. W.; Levy, D. H. *J. Chem. Phys.* **1997**, *106*, 10368.
(24) Elam, J. W.; Levy, D. H. *J. Appl. Phys.* **1997**, *81*, 539.
(25) Park, Y. D.; Rizzo, T. R.; Peteanu, L. A.; Levy, D. H. *J. Chem. Phys.* **1986**, *84*, 6539.
(26) Kelly, R.; Dreyfus, R. W. *Nucl. Instrum. Methods* **1988**, *B32*, 341.
(27) Menges, M.; Baumeister, B.; Al-Shamery, K.; Freund, H.-J.; Fischer, C.; Andresen, P. *Surf. Sci.* **1994**, *316*, 103.
(28) NoorBatcha, I.; Lucchese, R. R.; Zeiri, Y. *J. Chem. Phys.* **1987**, *86*, 5816.
(29) Voumard, P.; Zenobi, R. *J. Chem. Phys.* **1995**, *103*, 6795.
(30) Maechling, C. R.; Clemett, S. J.; Engelke, F.; Zare, R. N. *J. Chem. Phys.* **1996**, *104*, 8768.
(31) Zhan, Q.; Wright, S. J.; Zenobi, R. *J. Am. Soc. Mass Spectrom.* **1997**, *8*, 525.
(32) Kelly, R. *J. Chem. Phys.* **1990**, *92*, 5047.
(33) Kools, J. C. S.; Baller, T. S.; De Zwart, T. S.; Dieleman, J. *J. Appl. Phys.* **1992**, *71*, 4547. Kools, J. C. S.; van de Riet, E.; Dieleman, J. *J. Appl. Surf. Sci.* **1993**, *69*, 133.
(34) NoorBatcha, I.; Lucchese, R. R.; Zeiri, Y. *J. Chem. Phys.* **1988**, *89*, 5251.
(35) Wegener, P. *Molecular Beams and Low-Density Gas Dynamics*; M. Dekker: New York, 1974; Chapter 1.
(36) Kelly, R.; Cuomo, J. J.; Leary, P. A.; Rothenberg, J. E.; Braren, B. E.; Aliotta, C. F. *Nucl. Instrum. Methods* **1985**, *B9*, 329.
(37) Burgess, D., Jr.; Stair, P. C.; Weitz, E. *J. Vac. Sci. Technol., A* **1986**, *4*, 1362.
(38) Anderson, H. L. *A Physicists Desk Reference*; AIP: New York, 1989.
(39) Biondi, M. A.; Rayne, J. A. *Phys. Rev.* **1959**, *115*, 1522.
(40) Nagra, D. S.; Zhang, J. Y.; Wang, A. P. L.; Li, L. *Int. J. Mass Spectrom. Ion Processes* **1992**, *116*, 127.
(41) Walter, K.; Lindner, J.; Grotemeyer, J.; Schlag, E. W. *Chem. Phys.* **1988**, *125*, 155.
(42) Durant, J. L.; Rider, D. M.; Anderson, S. L.; Proch F. D.; Zare, R. N. *J. Chem. Phys.* **1984**, *80*, 1817.
(43) Levin, R. D.; Lias, S. G. *Ionization Potential and Appearance Potential Measurements, 1971−1981*; U.S. Government Printing Office: Washington, 1982.
(44) Benson, S. W.; Cruikshank, F. R.; Golden, D. M.; Haugen, G. R.; O'Neal, H. E.; Rodgers, A. S.; Shaw, R.; Walsh, R. *Chem. Rev.* **1969**, *69*, 279.
(45) Abel, B.; Herzog, B.; Hippler, H.; Troe, J. *J. Chem. Phys.* **1988**, *91*, 900.
(46) Hippler, H.; Troe, J.; Wendelken, H. J. *J. Chem. Phys.* **1983**, *78*, 6709.
(47) Rossi, M.; Pladziewicz, J. R.; Barker, J. R. *J. Chem. Phys.* **1983**, *78*, 6695.
(48) Steenvoorden, R. J. J. M.; van der Hage, E. R. E.; Boon, J. J.; Kistemaker, P. G.; Weeding, T. L. *Org. Mass. Spectrom.* **1994**, *29*, 78.
(49) Sibold, D.; Urbassek, H. M. *J. Appl. Phys.* **1993**, *73*, 8544.
(50) Venkatesan, T.; Wu, X. D.; Inam, A.; Wachtman, J. B. *Appl. Phys. Lett.* **1988**, *52*, 1193.